Electrical Impedance Tomography Based Finger-Shaped Soft Artificial Skin

Yunqi Huang[1], and Thomas George Thuruthel[1]

***Abstract*—Obtaining dense contact information for feedback control is vital for robotic manipulation. However, existing tactile sensing technologies have a large footprint, making seamless integration with current robotic devices difficult. This paper presents a novel multi-layer Electrical Impedance Tomography (EIT) sensor architecture designed to provide distributed, high-density tactile sensing with a small form factor. Using our multilayer structure, we address a common issue in other EIT-based tactile skins that prevents electrodes from being placed distally from the sensing surface. Our innovative multi-layer design enables the development of complex-shaped soft sensing skins without any electronic components on the sensing surface, achieving very high accuracy. To demonstrate practical applications, we fabricated a finger-shaped three-dimensional (3D) skin and conducted experiments to collect real-world data. We developed a perception model for the tactile sensor by employing data-driven machine learning methods to predict press localization and force with high accuracy based on EIT signals. Our work presents a significant step towards developing whole body full soft tactile sensors with a small form factor.**

***Index Terms*—Soft Sensors and Actuators, Force and Tactile Sensing.**

I. INTRODUCTION

In recent years, the deployment of robots has expanded significantly beyond traditional industrial applications. Robots are now increasingly utilized in diverse interactive tasks involving humans, real-world objects and complex environments. The sense of touch is going to play a central role in this advancement [1].

Tactile sensing, including the detection of pressure, strain, and slip, is a crucial perception mode for robots to perceive and navigate complex, unstructured environments [2]. Much like how human skin perceives external physical stimuli, flexible and stretchable electronic skins (or tactile skins) offer promising solutions to robotic sensing challenges [3], [4], [5].

Typically, tactile skins are developed using piezoresistive materials arranged in a grid structure [6], [7], [8], [9]. Similarly, discrete tactile units (taxels) can be created and distributed using capacitance-based sensors [10], [11] or pressure-based sensors [12], [13]. However, technologies based on individual taxel units present several challenges. First, due to their grid-like structure, wiring becomes complicated, with the number of electrodes scaling linearly with the number of taxels. This also reduces their stretchability, conformability, and robustness. Second, their spatial resolution is limited to the number of taxels, making scaling to large areas difficult.

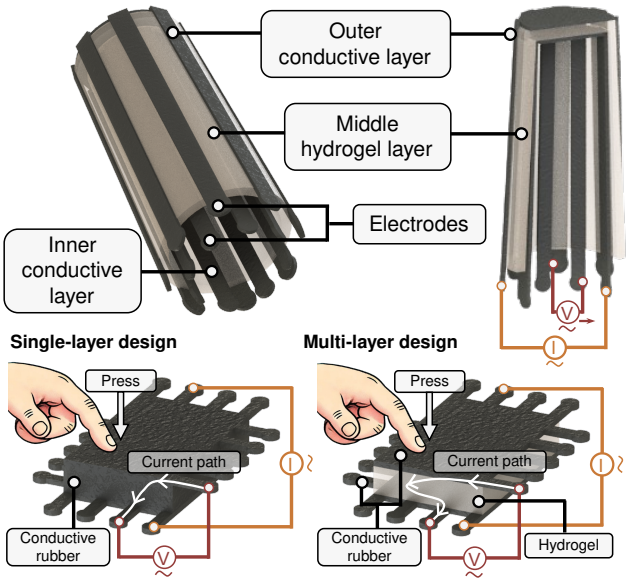

Fig. 1. Design and working principle of the multi-layer EIT-based finger-shaped soft artificial skin. The three-layer structure with 16 electrodes mounted at the base allows a convex shape of the skin. In the single-layer design (left), conductivity is uniform throughout the structure, resulting in poor pressure response. The multi-layer design (right) features varying conductivity with a low-conductivity middle layer, making the overall structure more sensitive to external pressure stimuli and improving tactile sensing capabilities.

Vision-based tactile skins are a promising route to address these issues [14], [15], but they still require a housing unit for the cameras near the skin. This increases their form factor and reduces their applicability. These challenges have led researchers to explore alternative approaches, among which Electrical Impedance Tomography (EIT) has gained significant attention [16], [17], [18].

EIT is a non-invasive medical imaging technique that provides continuous images of internal tissue conductivity by applying small currents and measuring voltages at the body surface [19]. It is well-suited for electronic skin and tactile sensing applications due to its ability to detect conductivity changes caused by physical interactions over large, flexible areas using only boundary and sparse electrodes [20], [21]. EIT-based tactile sensors offer several advantages including durability, large-area scalability, ease of fabrication, and a small form factor [17], [18]. The potential of EIT-based sensors have been demonstrated in various applications. These include soft robotic skins using ionically conductive hydrogels [18], and

Manuscript received: November 18, 2024; Revised: January 25, 2025; Accepted: March 25, 2025.

This paper was recommended for publication by Editor Yong-Lae Park upon evaluation of the Associate Editor and Reviewers' comments. This work was supported by the Royal Society research grant RGS/R1/231472.

Yunqi Huang and Thomas George Thuruthel are with Department of Computer Science, University College London, London, UK. yunqi.huang.23@ucl.ac.uk; t.thuruthel@ucl.ac.uk

Digital Object Identifier (DOI): see top of this page.

large-area flexible tactile sensors made from porous elastic polymers filled with ionic liquids [22] that can achieve tactile information reconstruction and ultrathin wearable electronics fabricated with hybrid materials and carbon nanotubes for human-machine interface [16]. Despite these advancements, EIT-based sensors still face challenges when implemented in complex morphologies, particularly in achieving high spatial resolution and optimal electrode placement in non-planar shapes [23].

To address these limitations, we present a novel multi-layer design for EIT-based artificial skin [23]. This design achieves enhanced sensitivity across three-dimensional (3D) geometries through its varying conductivity layers, generating distinct and robust signals throughout the sensing area that enable effective machine learning analysis. Based on this innovative approach, we have developed a finger-shaped artificial skin that is both soft and stretchable. The 3D skin has no electrodes on the sensing surface, offering high spatial resolution and the capability to detect contact locations and forces. Our extensive testing demonstrates the skin's stability and high sensitivity.

II. Theory

In the EIT-based tactile sensing skin system, the EIT technique is applied to a thin, soft, and stretchable conductive layer whose internal resistance responds to its physical deformation [24]. In the tactile skin system, a known current is injected through a pair of electrodes (source and sink), while voltages (electric potentials) are measured between non-current electrode pairs. This injected current generates an electrical potential distribution $\boldsymbol{u}$ across the conductive body Ω. The relationship between the potential distribution $\boldsymbol{u}$ and the body's internal impedance distribution σ is governed by the equation:

$$\nabla \cdot (\sigma \cdot \nabla \boldsymbol{u}) = 0 \quad in \quad \Omega \tag{1}$$

When external forces are applied to the skin, its internal impedance distribution σ changes as a function of contact information: position $(\mathbf{x},\mathbf{y})$ and force magnitude $\mathbf{F}$. The voltage measurements $\boldsymbol{u}$ from the remaining electrodes can be used to reconstruct this impedance distribution by solving the nonlinear inverse problem. A complete measurement cycle requires using all electrode combinations for current injection and voltage measurement. There are two main injection modes: adjacent and opposite [25]. In the adjacent mode, two injection electrodes are next to each other, while in the opposite mode, the two injection electrodes are separated by half the electrodes. The choice affects the measurement count per driving pair. For n electrodes skin, there are $(n-3)$ measurements for the adjacent mode and $(n-4)$ measurements for the opposite mode. This work employed adjacent current injections and adjacent measurements. By using the learning-based methods, this inverse problem can be formulated as a mapping function between the electrical measurements and contact information:

$$u = f(\sigma(\mathbf{x},\mathbf{y},\mathbf{F})) \tag{2}$$

where $f(\sigma())$ represents the nonlinear relationship that can be learned through data-driven methods.

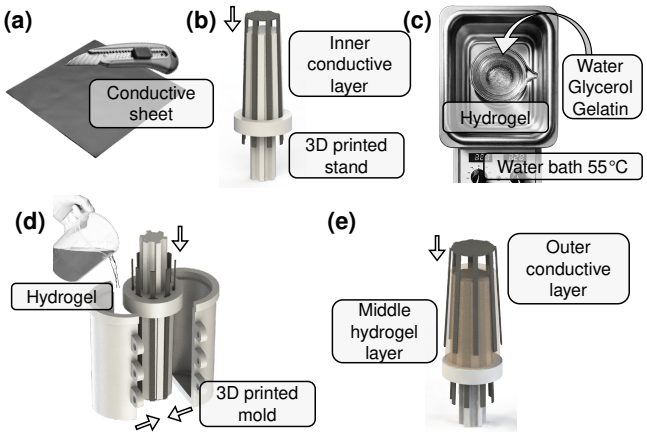

Fig. 2. Fabrication process of the finger-shaped soft artificial skin. (a) Cutting the conductive rubber sheet into the desired shape with eight elongated electrodes. (b) Placing the prepared inner conductive layer on the 3D-printed stand. (c) Preparing the hydrogel mixture in a 55°C water bath. (d) Pouring the hydrogel into the 3D-printed mold and carefully inserting the stand with the inner layer, ensuring even distribution of hydrogel on the surface. (e) After curing, removing the mold and applying the outer conductive layer over the hydrogel surface to complete the three-layer structure.

The sensitivity of the skin at different locations is determined by changes in electrical potential distribution upon touch. In single-layer EIT-based skins, the region of sensitivity diminishes as the distance from the injection and measurement electrodes increases, limiting their applicability to simple skin shapes with distributed electrodes. Scaling EIT-based technologies for complex skin surfaces with distal electrodes is feasible using multilayer architectures [23]. The key concept is to induce significant impedance changes upon contact by layering a high-impedance layer between two low-impedance, electrode-carrying layers (Fig. 1). Since the overall impedance of the multi-layer structure is high, determined primarily by the thin middle layer, any change in this layer (caused by touch) can significantly alter the current pathway. This enables the creation of complex-shaped, EIT-based tactile skins with distal electrodes.

III. Fabrication and Experiment

A. Skin Design and Fabrication

The fabrication of the finger-shaped soft artificial skin involves a multistep process, as illustrated in Fig. 2. This skin design consists of three primary layers: two conductive rubber sheets and one hydrogel layer sandwiched between them. The top and bottom layers are made of commercially available conductive rubber sheets (The Pi Hut, Conductive Rubber Sheet / Stretch Sensor). These sheets have high electrical conductivity, with a bulk sheet resistivity of approximately 70 ohm·mm in their relaxed state. The middle hydrogel layer is crafted by combining gelatin (sourced from pork), glycerol, and water in a precise ratio of 1:1.5:2.5 by weight, following the method described by Hardman et al. [26]. This mixture is heated in a water bath maintained at 55 °C. The assembly process utilizes custom 3D-printed polylactic acid (PLA) molds to place and shape the skin. The inner conductive layer is placed on a support, followed by pouring and curing the hydrogel middle

This article has been accepted for publication in IEEE Robotics and Automation Letters. This is the author's version which has not been fully edited and content may change prior to final publication. Citation information: DOI 10.1109/LRA.2025.3557297

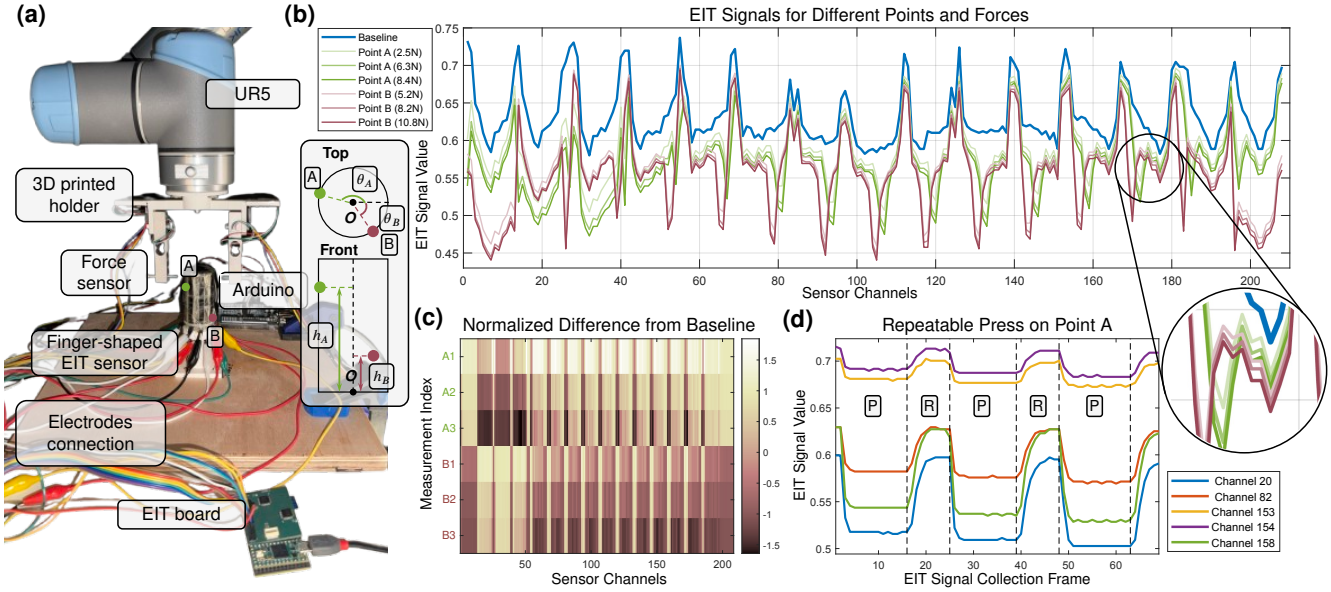

Fig. 3. (a) Experimental setup showing the finger-shaped soft skin pressed by a robotic arm equipped with force sensors. Key components include the EIT board and Arduino Mega 2560 for data collection. The sensor uses a cylindrical coordinate system (θ, h) (b) Raw EIT signals across 208 channels for presses on two different points (A and B) with varying forces. (c) Colored map showing the normalized difference from the baseline for different press localizations and forces. It corresponds to the raw signals shown in (b), with each row representing a different press condition. (d) Temporal visualization of EIT signals from selected channels during repeatable presses on point A, where 'P' indicates press and 'R' indicates release.

layer in the mold and finally applying the outer conductive layer. The finalized skin remains attached to the support for subsequent experimental tests. After assembly, the skin was wrapped with plastic tape to ensure consistent contact between the outer conductive layer and the middle hydrogel layer, as the hydrogel's adhesive properties degrade after thousands of press cycles.

The artificial skin's electrode configuration is designed to optimize sensing capabilities across its entire surface. Each conductive layer features 8 long strips that serve as electrodes, resulting in a total of 16 electrodes for the entire skin structure. Furthermore, the electrodes on the upper and lower conductive layers are positioned in an interlaced pattern. This arrangement guarantees that the whole skin is effectively 'wrapped' by the conductive layers, creating a continuous sensing field throughout the structure. By placing all the electrodes at the base of the artificial skin, this design allows for the creation of more complex and diverse skin shapes. The base-mounted electrodes leave the rest of the skin's surface free from rigid components, it can bend, stretch, and compress freely. This conformability is essential for applications where the sensor needs to wrap around robots' joints or cover irregular surfaces.

B. Hardware Setup

The experimental hardware setup is illustrated in Fig. 3 (a). The fabricated finger-shaped artificial skin, secured in its custom 3D-printed support, is fixed to a flat table. A UR5 robotic arm is used to apply precise pressure at various points on the skin's surface. Attached to the end-effector are force sensors (Sparkfun TAL220 Series Parallel Beam Load Cell) to measure the applied force accurately. Besides, an M4 screw is affixed to the bottom of the force sensor as the press probe, providing a 4 mm diameter pressing surface.

The electrodes of the artificial skin are connected to a specialized EIT board [27], which is capable of injecting alternating current (AC) into the skin and measuring the voltages between electrode pairs. The board provides adjustable AC current injection using a signal generator (AD5930) with output voltages ranging from -5 V to 5 V at a frequency of 20 KHz. An ADC converter performs voltage measurements at a 20 MHz sampling rate. We oversampled the impedance measurements to reduce noise. Each frame was obtained at 2.2 Hz

The electrodes on the upper conductive layer are connected to odd-numbered pins on the EIT board, while those on the lower layer are connected to even-numbered pins. This alternating connection ensures that adjacent voltage measuring pairs on the EIT board always span the entire three-layer structure of the artificial skin. In this way, each measurement can capture the conductivity changes across all layers, including the middle hydrogel layer. This design significantly enhances the sensor's sensitivity to impedance variations throughout the entire structure. The force sensors are connected to an Arduino Mega 2560 microcontroller via the amplifier (SparkFun Load Cell Amplifier - HX711). This setup allows for real-time force data collection alongside the EIT measurements.

C. Raw Data Visualization

The working principle of the EIT-based soft artificial skin is illustrated in Fig. 1. This skin has a configuration of 16 electrodes and its data collection occurring in discrete frames. For each frame, a driving current is applied to a specific pair of electrodes, highlighted in orange. Simultaneously, the

board measures potential differences across all other adjacent remaining electrode pairs, denoted in red. There are two methods for selecting the driving electrodes: adjacent and opposite. In the adjacent mode, the driving electrodes are next to each other, while in the opposite mode, the driving electrodes are separated by 7 intervening electrodes in this configuration. The choice of mode affects the number of measurements taken per driving pair: 13 for adjacent mode and 12 for opposite mode. In this experiment, we employed the adjacent mode, which results in a total of $16 \times 13 = 208$ valid measurements in each collection frame.

Fig. 3(b) shows the raw EIT signals for the soft artificial skin at rest (baseline) and during presses at two different points (A and B) with varying forces. The data reveals unique signal patterns for different press localizations, demonstrating the skin's ability to differentiate spatial stimuli. Moreover, for each localization, the signal deviation from the baseline correlates with the applied force magnitude, indicating its force sensitivity. The signal difference for these presses is visualized as a colored map in Fig. 3(c). The contrasting patterns for points A and B further illustrate the skin's spatial discrimination capability, while the increasing color intensity with higher force applications (e.g., from A1 to A3) confirms the skin's ability to discern force magnitudes. To evaluate the repeatability of the skin's response, Fig. 3(d) shows the temporal change of signals from selected channels during multiple press-release cycles at point A. Channels 20, 82, and 158 exhibit clear and significant responses to the applied pressure while channels 153 and 154 show minimal reactivity to this localization press.

This analysis demonstrates three key properties of the EIT-based soft artificial skin: spatial sensitivity, which can generate unique signal patterns for different press localizations; force sensitivity, the signal deviation from the baseline correlates strongly with the applied force; and repeatability, which exhibits consistent signal patterns for repeated stimuli at the same localization. Furthermore, the clear and consistent relationship between EIT signals and both localization and force inputs provides a solid foundation for advanced data analysis techniques. This proves the feasibility of the subsequent work: collecting a comprehensive dataset for training a neural network to predict touch location and force based on the raw EIT signals.

D. Data Collection and Neural Network Training

The data collection process involves EIT signal acquisition, robotic arm movement, press force measurement and their synchronization. The objective of the process is to gather comprehensive data on the artificial skin's response to various pressure stimuli on its surface. Firstly, a dedicated thread continuously reads EIT signals from the sensor at a frequency of 2.2 Hz through the USB connection of the EIT board and the PC. Each reading is timestamped for later alignment. The robotic arm control thread executes a four-state movement cycle for each target data point.

- Move: A cylindrical coordinate of the target point $(\theta, \mathbf{h})$ on the sensor's surface is generated. The arm moves the probe to a plane just the same height as this point.

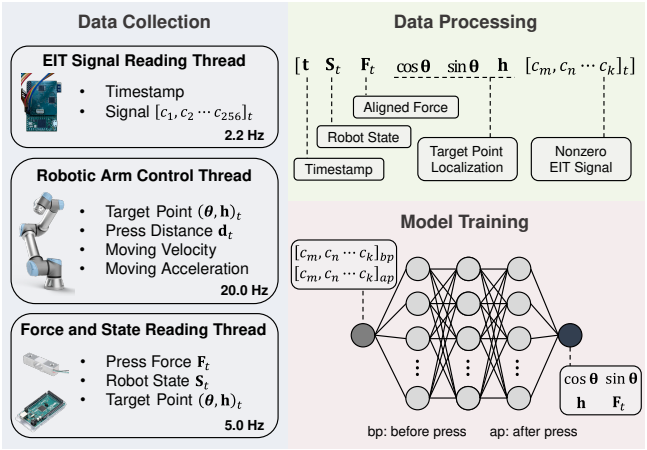

Fig. 4. Data Collection, processing, and model training pipeline for the finger-shaped soft artificial skin. The left side illustrates the multithreaded data collection. The right side shows the data processing, aligning, and transforming to a structured format for neural network training.

- Press: The end-effector moves horizontally, using the probe to press on the target point. The press distance $\mathbf{d}$ is randomized within a predetermined range to vary the applied force across trials.
- Hold: The probe maintains its position for 3 seconds, ensuring stable pressure is applied and allowing the sensor to reach a steady-state response.
- Release: The probe is lifted from the sensor surface.

This cycle is then repeated with the opposite probe and sensor, providing complete data collection across the entire sensor surface. During the arm movement cycle, force readings from the sensors $(\mathbf{F}_t)$ are recorded at a frequency of 5 Hz. These readings are timestamped $(\mathbf{t})$ and paired with the current robotic arm state $\mathbf{S}_t$ (move, press, hold, or release) and the target point coordinate $(\theta, \mathbf{h})_t$.

After collection, the data undergoes several processing steps to be prepared for model training. To align the EIT signal with the robot movement and force readings, the force data is first resampled to 20 Hz using linear interpolation. This matches the frequency of the robotic arm control thread. The EIT readings, originally collected at 2.2 Hz, are then aligned with their nearest corresponding force measurements, target localizations, and robotic arm states based on timestamps. The angular component θ of the localization element is converted to its sine and cosine to avoid discontinuities and ambiguities for the model training process. For each EIT data collection cycle, the EIT board yields 256 sets of voltage measurement data, while some measurements from electrodes serving as current sources are set to 0. The final EIT signal frame comprises 208 non-zero signal sets, denoted as $[c_m, c_n, \ldots c_k]$. The final data frame structure, as illustrated in Fig. 4, includes the timestamp, robot state, aligned force, transformed target point localization, and the non-zero EIT signals.

For the neural network training, the data is organized into input-output pairs. The input consists of 416 features, representing the EIT signals before and during the press state. The output corresponds to the transformed target point localization

This article has been accepted for publication in IEEE Robotics and Automation Letters. This is the author's version which has not been fully edited and content may change prior to final publication. Citation information: DOI 10.1109/LRA.2025.3557297

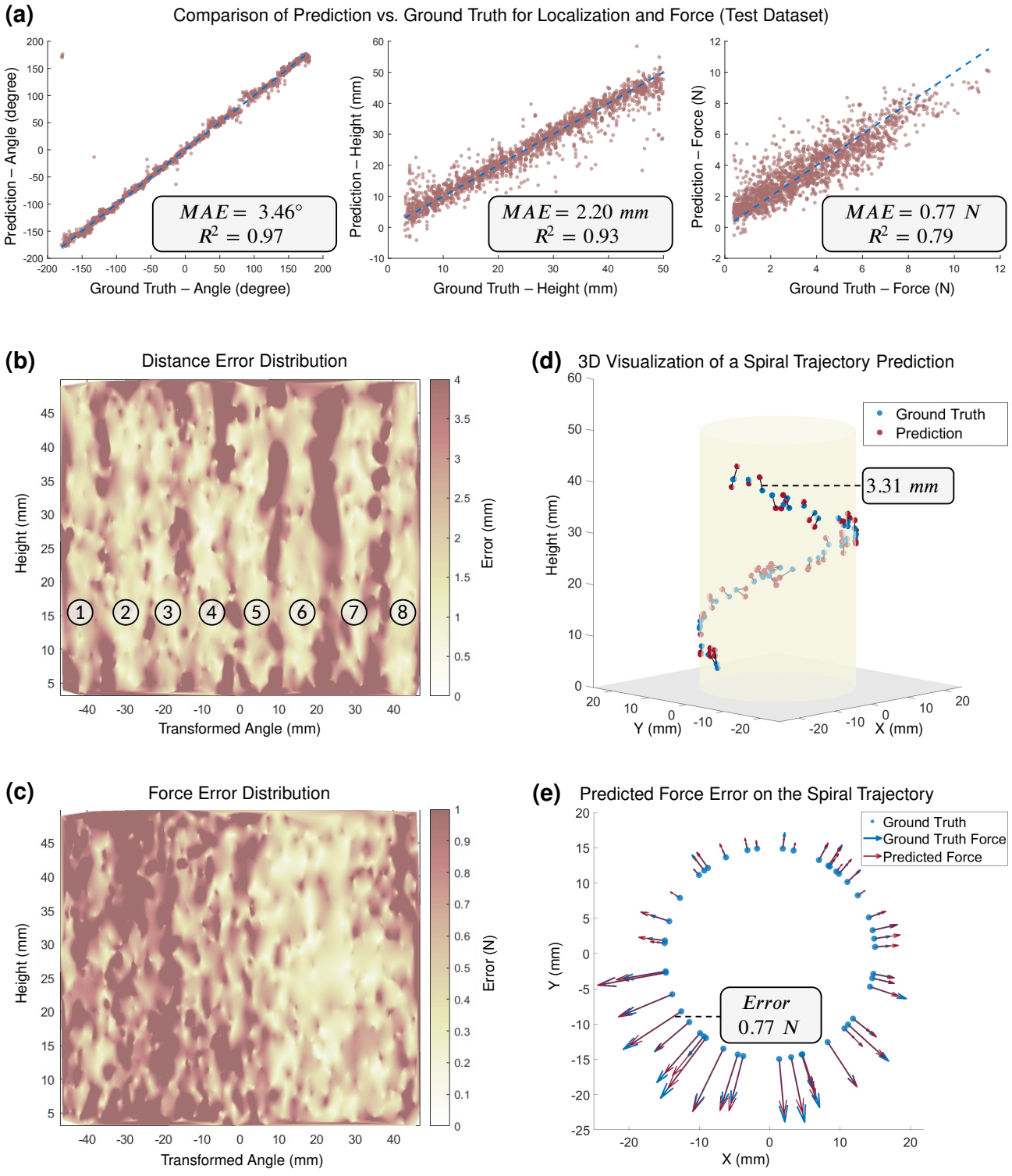

Fig. 5. Analysis of our perception model. (a) Scatter plots comparing predicted vs. ground truth values for localization (angle and height in cylindrical coordinates) and force, with their Mean Absolute Error (MAE) and R^2 values. R^2 ranges from 0 to 1, where 1 indicates a perfect fit. (b),(c) Colored maps representing the unrolled surface of the cylindrical skin, showing the spatial distribution of distance and force prediction errors, respectively. (d) 3D visualization of predicted (red) and ground truth (blue) points along a spiral trajectory on the skin surface. (e) Top view of the force prediction errors along the spiral trajectory, with arrows indicating the ground truth (blue) and predicted (red) forces' magnitude.

and force. The neural network architecture comprises an input layer of 416 nodes, followed by three hidden layers with 300, 50, and 20 nodes respectively, and a 4-node regression output layer. The complete dataset consists of 1,900 presses totaling 22,858 data frames, which are split into training, validation, and test (80%, 10%, 10%) sets. Training (using stochastic gradient descent with momentum) begins with a learning rate of 0.005 and a batch size of 1,024.

IV. Results

A. Localization and Force Prediction

We evaluated the performance of the trained neural network for predicting press localization and applied force magnitude. Fig. 5(a) shows the comparison between predicted and ground truth values for angle, height, and force. The results demonstrate effective prediction performance, particularly in localizing press points. For localization, the high R^2 values for angle and height indicate a strong correlation between the predicted and actual values. The Mean Absolute Errors (MAE) further confirm the high accuracy. To put the localization accuracy into perspective, we calculated the average distance error on the unrolled surface of the cylindrical skin is **2.74** mm. This level of precision is particularly impressive when considering that the pressing probe used in our experiments is an M4 screw with a 4 mm diameter.

While force prediction accuracy is reasonably with an average error of **0.77** N over a 10 N force range, the R^2 values suggest that estimating applied force is more challenging than determining press localization for the trained model. One reason for this could be the complex nonlinear behaviour of our sensing material, which would require more dynamic data to be more informative. Hence, a higher sampling rate is imperative for better force estimation. The comprehensive visualizations in Fig. 5(d-e) provide additional insights into the localization and force prediction along a spiral trajectory on the sensor surface. These visualizations further validate the trained neural network's capability to accurately predict press points and estimate forces in various locations.

B. Error Distribution Map Analysis

Fig. 5(b-c) presents unrolled surface maps of the cylindrical skin, the interpolated colored maps illustrate the spatial distribution of distance and force prediction errors. We employed MATLAB's 'natural' scatter interpolation method to get these continuous error distribution maps. This natural-neighbor interpolation method produces a C1 continuous surface except at the sample points, offering a smooth representation of error variation across the surface.

The distance error map shows an intriguing pattern of eight linear regions with high prediction accuracy. These regions correspond precisely to the locations of the eight long strip electrodes on the outer conductive layer of the skin. This observation reveals that the areas directly above the electrodes probably have higher sensitivity to conductivity changes. It also suggests that increasing the number and density of electrodes could potentially enhance overall prediction accuracy across the entire skin surface.

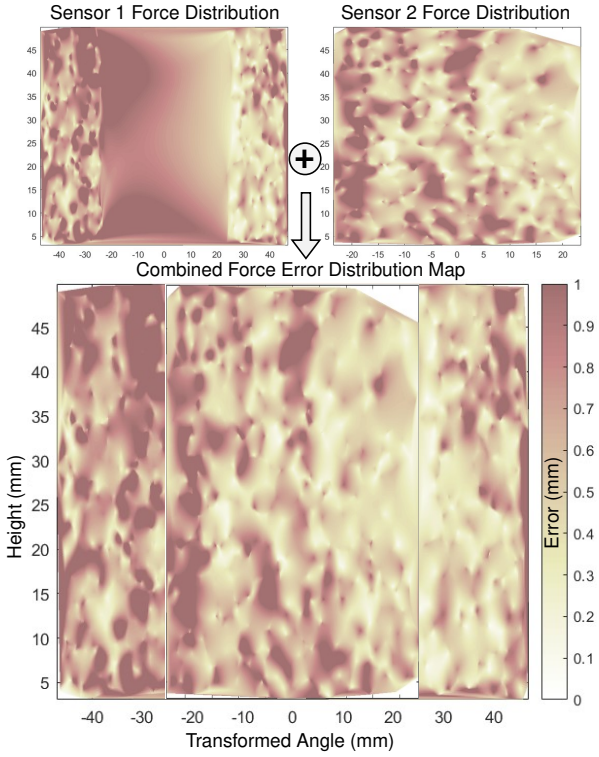

Fig. 6. Comparison of force prediction errors using sensor-specific training. The top two are individual error distribution maps for each sensor. The bottom combined force error distribution map showing improved accuracy and uniformity compared to the single-model approach

The force error distribution map shows a non-uniform pattern across the sensor surface, while the right half has higher prediction accuracy. This uneven distribution can be attributed to factors in both the fabrication process and the experimental setup. During the skin's fabrication, the stand is inserted into a mold filled with hydrogel, which then cures to form the middle layer. However, the stand is not always positioned perfectly at the center of the mold, resulting in an uneven distribution of the hydrogel middle layer around the surface. This non-uniform thickness of the middle layer could lead to variations in force sensitivity across the skin. Additionally, the press data collections are done by two force sensors, each covering half of the skin's surface. The skin stand is not perfectly centered between the two force sensors, potentially leading to systematic differences in force measurements across the surface.

C. Improved Force Prediction by Sensor-Specific Training

To address the non-uniform force prediction accuracy observed in the initial analysis and to minimize the influence of fabrication inconsistencies and experimental setup variations, we implemented a sensor-specific training approach. Instead of training a single model with combined data, we separated the dataset based on the two force sensors (SparkFun TAL220) used in data collection and trained individual models for each sensor's measurements. The results of this approach are illustrated in Fig. 6.

As shown in Fig. 6, Sensor 2 demonstrates better prediction accuracy compared to Sensor 1. This difference reveals that the area covered by Sensor 2 likely has a more uniform hydrogel layer distribution. Our final observation of the skin after the experiment confirmed this hypothesis, showing that this side indeed has a thicker and even hydrogel layer. Comparing the combined distribution map with Fig. 5(c), which was based on a single model trained with data from both sensors, this sensor-specific training shows a marked improvement in overall accuracy with $MAE = 0.65$ N (14.7% improvement). These results highlight the importance of considering individual sensor characteristics and local structural variations in the training process. By accounting for the unique properties and positioning of each force sensor, as well as potential inconsistencies in the skin's fabrication, we are able to achieve more accurate and consistent force predictions across the entire surface of the artificial skin.

V. Conclusion

In this paper, we presented a novel multi-layer EIT-based soft sensor architecture designed for distributed high-density tactile sensing of complex shapes. Our 3D finger-shaped soft artificial skin with innovative design demonstrates remarkable stability and robustness over thousands of press cycles, with the perception model achieving high accuracy in tactile information prediction. The novel multi-layer design plays a crucial role in enhancing its sensitivity to external pressure. By incorporating multiple layers with varying conductivity (hydrogel and conductive rubber), the skin structure responds more distinctly to applied forces, resulting in more complex and informative EIT signals. Using the machine learning method, the 3D tactile information can be extracted from the EIT signals with much higher accuracy than existing EIT-based tactile sensors, achieving **2.74** mm average localization error and **0.77** N force prediction error. While the current results were achieved using a 4 mm diameter M4 screw as a probe, performance could be further improved via enhanced data collection protocols, larger datasets, and refined neural network architectures. Besides, the base-mounted electrode placement enables a continuous and fully soft cylindrical sensing area. This sensing technology has potential applications in robotic manipulation and human-robot interaction where precise tactile feedback is crucial. The flexible design allows it to cover complex geometries such as robotic hands, joints and limbs, to provide stable and accurate tactile sensing and perception for delicate manipulation and safe interactions.

Our work faces several limitations. The hydrogel middle layer's susceptibility to water loss degrades the sensor's press response sensitivity after three months of use. Future work will explore more stable layer materials and improved sealing methods, such as additional silicone encapsulation, to extend the sensor's lifespan. The static perception model also presents limitations. Each prediction cycle (press-response-collection-prediction) takes approximately 3 seconds, limiting dynamic performance in real-time tactile sensing. The insights gained from distance and force error distribution maps point towards specific strategies for enhancing the sensor's performance in future iterations. Refining the fabrication process to ensure more uniform hydrogel distribution could enhance consistency in force sensitivity. Additionally, exploring increased electrode densities and alternative electrode configurations could potentially lead to even higher accuracy in both localization and force prediction.

References

[1] M. M. Lee, "Tactile sensors need a greater sense of purpose," *Science Robotics*, vol. 7, no. 63, p. eabn9086, 2022.

[2] R. S. Dahiya, G. Metta, M. Valle, and G. Sandini, "Tactile sensing—from humans to humanoids," *IEEE transactions on robotics*, vol. 26, no. 1, pp. 1–20, 2009.

[3] R. Dahiya, N. Yogeswaran, F. Liu, L. Manjakkal, E. Burdet, V. Hayward, and H. Jörntell, "Large-area soft e-skin: The challenges beyond sensor designs," *Proceedings of the IEEE*, vol. 107, no. 10, pp. 2016–2033, 2019.

[4] B. Shih, D. Shah, J. Li, T. G. Thuruthel, Y.-L. Park, F. Iida, Z. Bao, R. Kramer-Bottiglio, and M. T. Tolley, "Electronic skins and machine learning for intelligent soft robots," *Science Robotics*, vol. 5, no. 41, p. eaaz9239, 2020.

[5] M. Amjadi, K.-U. Kyung, I. Park, and M. Sitti, "Stretchable, skin-mountable, and wearable strain sensors and their potential applications: a review," *Advanced Functional Materials*, vol. 26, no. 11, pp. 1678–1698, 2016.

[6] K. Kim, K. R. Lee, W. H. Kim, K.-B. Park, T.-H. Kim, J.-S. Kim, and J. J. Pak, "Polymer-based flexible tactile sensor up to 32× 32 arrays integrated with interconnection terminals," *Sensors and Actuators A: Physical*, vol. 156, no. 2, pp. 284–291, 2009.

[7] S. Lee, A. Reuveny, J. Reeder, S. Lee, H. Jin, Q. Liu, T. Yokota, T. Sekitani, T. Isoyama, Y. Abe *et al.*, "A transparent bending-insensitive pressure sensor," *Nature nanotechnology*, vol. 11, no. 5, pp. 472–478, 2016.

[8] S. Sundaram, P. Kellnhofer, Y. Li, J.-Y. Zhu, A. Torralba, and W. Matusik, "Learning the signatures of the human grasp using a scalable tactile glove," *Nature*, vol. 569, no. 7758, pp. 698–702, 2019.

[9] Y. Luo, Y. Li, P. Sharma, W. Shou, K. Wu, M. Foshey, B. Li, T. Palacios, A. Torralba, and W. Matusik, "Learning human–environment interactions using conformal tactile textiles," *Nature Electronics*, vol. 4, no. 3, pp. 193–201, 2021.

[10] D. Hughes, J. Lammie, and N. Correll, "A robotic skin for collision avoidance and affective touch recognition," *IEEE Robotics and Automation Letters*, vol. 3, no. 3, pp. 1386–1393, 2018.

[11] K.-H. Ha, H. Huh, Z. Li, and N. Lu, "Soft capacitive pressure sensors: trends, challenges, and perspectives," *ACS nano*, vol. 16, no. 3, pp. 3442–3448, 2022.

[12] T. Kim, J. Park, S. J. Yoon, H.-W. Park, Y.-L. Park *et al.*, "Design of a lightweight inflatable sensing sleeve for increased adaptability and safety of legged robots," in *2019 2nd IEEE International Conference on Soft Robotics (RoboSoft)*. IEEE, 2019, pp. 257–264.

[13] K. Gilday, T. George-Thuruthel, and F. Iida, "Predictive learning of error recovery with a sensorized passivity-based soft anthropomorphic hand," *Advanced Intelligent Systems*, vol. 5, no. 7, p. 2200390, 2023.

[14] B. Ward-Cherrier, N. Pestell, L. Cramphorn, B. Winstone, M. E. Giannaccini, J. Rossiter, and N. F. Lepora, "The tactip family: Soft optical tactile sensors with 3d-printed biomimetic morphologies," *Soft robotics*, vol. 5, no. 2, pp. 216–227, 2018.

[15] L. Van Duong *et al.*, "Large-scale vision-based tactile sensing for robot links: Design, modeling, and evaluation," *IEEE Transactions on Robotics*, vol. 37, no. 2, pp. 390–403, 2020.

[16] H. Chen, X. Yang, P. Wang, J. Geng, G. Ma, and X. Wang, "A large-area flexible tactile sensor for multi-touch and force detection using electrical impedance tomography," *IEEE Sensors Journal*, vol. 22, no. 7, pp. 7119–7129, 2022.

[17] W. Xin, F. Zhu, P. Wang, Z. Xie, Z. Tang, and C. Laschi, "Electrical impedance tomographic shape sensing for soft robots," *IEEE Robotics and Automation Letters*, vol. 8, no. 3, pp. 1555–1562, 2023.

[18] D. Hardman, T. G. Thuruthel, and F. Iida, "Tactile perception in hydrogel-based robotic skins using data-driven electrical impedance tomography," *Materials Today Electronics*, vol. 4, p. 100032, 2023.

[19] S. H. Yoon, K. Huo, Y. Zhang, G. Chen, L. Paredes, S. Chidambaram, and K. Ramani, "isoft: a customizable soft sensor with real-time continuous contact and stretching sensing," in *Proceedings of the 30th Annual ACM Symposium on User Interface Software and Technology*, 2017, pp. 665–678.

[20] J.-B. Chossat, H.-S. Shin, Y.-L. Park, and V. Duchaine, "Soft tactile skin using an embedded ionic liquid and tomographic imaging," *Journal of mechanisms and robotics*, vol. 7, no. 2, p. 021008, 2015.

[21] S. Russo, S. Nefti-Meziani, N. Carbonaro, and A. Tognetti, "A quantitative evaluation of drive pattern selection for optimizing eit-based stretchable sensors," *Sensors*, vol. 17, no. 9, p. 1999, 2017.

[22] K. Kim, J.-H. Hong, K. Bae, K. Lee, D. J. Lee, J. Park, H. Zhang, M. Sang, J. E. Ju, Y. U. Cho *et al.*, "Extremely durable electrical impedance tomography–based soft and ultrathin wearable e-skin for three-dimensional tactile interfaces," *Science Advances*, vol. 10, no. 38, p. eadr1099, 2024.

[23] Y. Wang, D. Naritomi, H. Shigemune, and T. G. Thuruthel, "Multi-layer electrical impedance tomography based soft tactile skins," in *2024 IEEE 7th International Conference on Soft Robotics (RoboSoft)*. IEEE, 2024, pp. 1101–1106.

[24] D. Silvera-Tawil, D. Rye, M. Soleimani, and M. Velonaki, "Electrical impedance tomography for artificial sensitive robotic skin: A review," *IEEE Sensors Journal*, vol. 15, no. 4, pp. 2001–2016, 2015.

[25] O. Luppi Silva, R. Gonzalez Lima, T. Castro Martins, F. Silva de Moura, R. Seiji Tavares, and M. Sales Guerra Tsuzuki, "Influence of current injection pattern and electric potential measurement strategies in electrical impedance tomography," *Control Engineering Practice*, vol. 58, pp. 276–286, 2017.

[26] D. Hardman, T. George Thuruthel, and F. Iida, "Self-healing ionic gelatin/glycerol hydrogels for strain sensing applications," *NPG Asia Materials*, vol. 14, no. 1, 12 2022.

[27] J. Zhu, J. C. Snowden, J. Verdejo, E. Chen, P. Zhang, H. Ghaednia, J. H. Schwab, and S. Mueller, "EIT-kit: An Electrical Impedance Tomography Toolkit for Health and Motion Sensing," in *UIST 2021 - Proceedings of the 34th Annual ACM Symposium on User Interface Software and Technology*. Association for Computing Machinery, Inc, 10 2021, pp. 400–413.